Primary System Transient Heating in a Severe Accident Scenario

M. di Marzo[1], M.A. Salehi[2] and K. Almenas[3]

The transient heat-up of a B&W PWR nuclear plant during core uncovery is investigated experimentally. For these conditions, circulation in the primary system is blocked by liquid water in the lower portion of the steam generators and in the cold legs pump suction risers. A scaled test facility including the reactor vessel, the hot legs up to the steam generators and the cold legs up to the pump discharge is used to infer transient temperature excursions at potential failure points in the system (i.e., the pressurizer surge line nozzle at the hot leg). The timing and nature of these failures determine the subsequent direct containment heating scenarios.

In this paper, emphasis is placed on the hot legs. The relevant scaling parameters are derived from the mass, momentum and energy equations for the hot legs and from the energy equation for the hot leg metal wall. The prototypical behavior for a given set of conditions is deduced from a multiple series of tests. This procedure is based on the concept ramp ratio concept. This parameter is defined as the ratio of the temperature ramps for the prototype and for the model. The predictions of the prototypical behavior are weighted against the model scaling distortions to assess their significance. An overall description of the transient temperature distribution of the fluid in the upper head and the hot leg metal wall at the surge line for various system operating powers, as well as the energy transport between the core and the various system elements, is provided. The paper also describes the main features of the single phase counter-current flow in the horizontal portion of the hot legs, where an attempt is made to deduce the transient velocity distribution from the measured temperature profiles.

INTRODUCTION

One of the hypothetical scenarios of a severe nuclear power plant accident is Direct Containment Heating (DCH) where, during a core melt event, the pressure of the primary system is maintained and a breach is created at the reactor vessel bottom. As a result, a violent expulsion of the dispersal molten corium into the containment leads to rapid transfer of mass and energy to the containment atmosphere due to the molten corium dispersal.

Recently it has been postulated [1-4] that the primary system may depressurize prior to a failure in the bottom section of the pressure vessel due to a failure in the upper region of the primary system. Sheron [2] showed that the evaluation of the probability of DCH occurrence is based on expert judgment, but not on actual experience or data. Thus, experimental data

1. Department of Mechanical Engineering, University of Maryland, College Park, MD 20742.
2. Department of Mechanical Engineering, Sharif University of Technology, Tehran, I.R. Iran.
3. Department of Material and Nuclear Engineering, University of Maryland, College Park, MD 20742.

Scientia Iranica, Vol. 2, No. 1, © Sharif University of Technology, March 1995.

for flow geometries and operating conditions simulating those above the degraded core are needed. In order to obtain scaled data for the prototype, it is required to transpose experimental data through appropriate scaling.

Allison [1] and Denny [5] summarized a number of experimental and analytical results. Stewart [6,7] and co-workers conducted a series of experiments on a 1/7 test facility at Westinghouse to approximate the hot leg flow geometries of a B&W plant. Analytical studies have been carried out using the current state-of-the-art thermal hydraulic codes such as RELAP5 [8], SCADAP/RELAP5 [9] and the CORMELT [5].

All previous scaling studies focused on the fluid within the system and provided a simplified treatment of the metal structures. A steady or quasi-steady state is assumed so that the contribution of the solid structures heat capacities can be neglected. Wassel [10] handled solid structures using the lumped parameter approximation. Recently, Tung [11] reviewed the scaling used by Westinghouse, and No and Ishii [12] addressed the heat up transient of the core region. A scaling rational for primary system transient heating was proposed by di Marzo [13]. The study provides a detailed scaling of the hot legs and a methodology which could be used to infer the transient thermal behavior of the hot leg metal.

For experiments that seek to quantify the energy transport above a degraded core, the effect of energy transport by radiation is an additional unique issue. This effect cannot be reproduced in low temperature experimental facilities, but its influence must be considered. Ostrach [14] showed that steam will be largely opaque to thermal radiation and most regions within the primary will be optically thick at high pressure and temperature conditions.

EXPERIMENTAL FACILITY

The experimental measurements are to be performed on the existing University of Maryland at College Park (UMCP) experimental thermal-hydraulic facility, where the UMCP integral test facility is a comprehensive, scaled representation of a B&W PWR system. Originally, the facility consisted of two complete loops, each incorporating a hot leg, once through steam generator (OTSG) and two cold legs. The pressure vessel includes a circumferential downcomer, upper plenum, upper head and eight reactor vessel vent valves connecting the downcomer and upper plenum regions at an elevation above the hot leg penetration. For the current test program, the facility was modified according to the scaling approach outlined in references [13] and [15].

The experiments were conducted under the assumption that fluid inventory in the plant is lost to the extent that the core uncovers. Normal system recirculation flow will be blocked by water collected in the lower half of the steam generators and cold legs and also in the bottom portion of the vessel, which is shown in Figure 1. The entire upper part of the system will be filled with steam and, as the accident progresses, by a superheated steam-hydrogen mixture.

This paper is to provide an energy transport for a system configuration and information concerning the transient metal temperature in the hot leg at the pressurizer surge line noz-

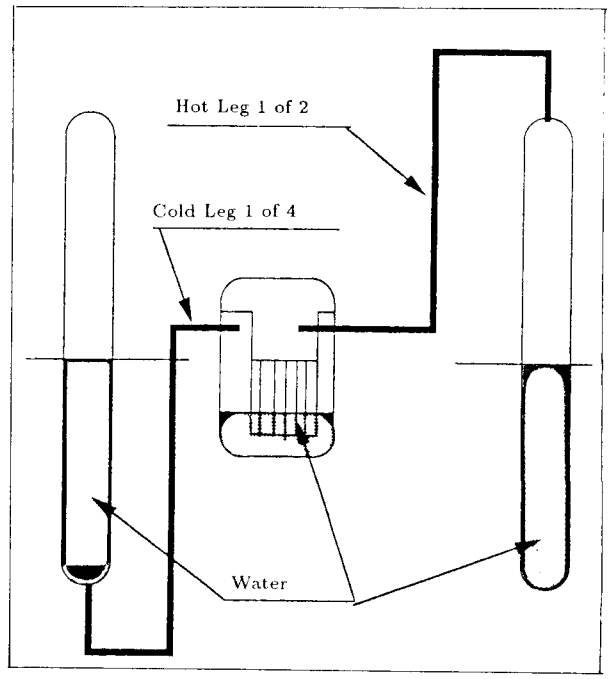

Figure 1. Primary system schematic.

Table 1. Prototypical and model physical properties and representative dimensions.

	Prototype	**Model**	**P/M**
Fluid	H_2O & H_2	SF_6	
System Pressure (MPa)	7.0 - 14	2.0	
System Temperature (C)	300 - 1300	20 - 190	
Ambient Temperature (C)	100	20	
Fluid Density (kg/m^3)	25	120	0.21
Fluid Viscosity (kg/m–s)	3.4e - 5	2.0e - 5	1.7
Fluid Thermal Cond. (W/m–K)	0.10	0.019	5.3
Fluid Specific Heat (J/kg–K)	3.4e + 3	8.4e + 2	4.1
Fluid Thermal Expan. Coeff. (1/K)	1.7e - 3	5.3e - 3	0.32
Hot Leg Length (m)	21	1.6	13
Hot Leg Inside Diameter (m)	0.91	0.087	11
Hot Leg Wall Thickness (m)	0.070	0.014	5.0

zle, where failure could be expected, and to estimate time-to-failure to be compared with estimates for the vessel lower head failure. The maximum operating pressure and the temperature for the facility are 20 bars and 500°C, respectively. The fluid used to simulate the high pressure steam is SF_6. Table 1 lists the geometrically averaged fluid properties during the transient, some of the hot legs geometrical characteristics for the prototype and for the model, the pressure and temperature range of the prototype and model and the prototype to model ratios.

The main instrument part which is required for the experiments is the Data Acquisition System (DAS), which samples 170 thermocouples (TCs). DAS has two separate sub-systems. HP-3852 DAS, which samples 144 channels at 100 kHz and HP-3497 Controller/DAS, which samples 25 channels at 6 kHz and also controls the 19 heaters. The two DAS systems are independent during operation, but information can be transferred from both devices to an IBM PS-2/386SX, which is used to process and store the data [16].

The pressure vessel has been extensively instrumented with TCs (84 TCs). This large number of TCs was required, since the flow geometry and patterns in the vessel were not quantified. The two hot legs are equipped with TCs sampling the metal and the fluid temperature. In addition, the fluid TCs are arranged inside the hot leg to provide the gages temperature distribution in the leg.

Power at the facility is generated by 19 heaters, each with a capacity of 3 kW. The power is applied on demand from DAS to the heaters. The accuracy of power measurement is desired to be within 2 percent of the full power (57 kW). The power measurement has direct relation with the heat transfer coefficient estimation and power ramps of the scaling methodology. The power ramps are required for the estimation of time-to-failure of the prototype (i.e., surge line).

There are two pressure transducers available for the experiments, where in each experiment the pressure of the system is kept constant. The pressure transducers are connected to one of the cold legs.

As the hot gas moves up the hot leg, it loses energy to the metal of the hot leg and, thus, cools off. Since the top of the hot leg is closed, the gas has to reverse direction. The point where the gas reverses direction could be anywhere in the hot leg, depending upon the

energy of the gas. This flow reversal is assumed to present a flow of the hot gas up in the center of the hot leg and return of the cooler gas down around the edges of the hot leg.

The counter-current flow in the hot leg sleeve is observed and the flow associates the energy and mass transport to the hot leg and the surge line. Note that the amount of energy carried by the fluid to the hot leg metal wall and the surge line will be estimated. The velocities in the hot leg sleeve are obtained from the experimental measurement of temperatures in 10 TCs in the hot leg sleeve and also using the energy equation applied for the horizontal portion of the hot leg. Temperature difference of up to 7°C in the 10 cm gap and ΔT of 50-70°C in the vertical locations (top to bottom) are observed.

SCALING

The objective of this scaling effort is to find a sound methodology to translate measurement obtained in a scaled model to prototypical conditions. The emphasis of this paper is to describe power and mass transfer phenomena in the hot leg and the scaling of the transient thermal behavior of metal at remote locations.

The conservation of momentum and energy equations for the fluid in the hot legs and the energy equation for the metal wall, using a lumped capacity approximation for the metal and the Boussinesq approximation for the fluid, are as follow:

$$\frac{\partial \vec{u}}{\partial t} + \nabla.(\vec{u}\vec{u} - \nu\nabla\vec{u}) = \beta\Delta T\vec{\gamma}g \ , \tag{1}$$

$$\frac{\partial T}{\partial t} + \nabla.(\vec{u}T - \alpha\nabla T) = 0 \ , \tag{2}$$

$$(\rho c)_m \frac{dT_m}{dt} = -\nabla.[K(\frac{\partial T}{\partial y_{@wall}}) + h_e(T_m - T_\infty)]\hat{n} \ , \tag{3}$$

where $\vec{\gamma}$ is a vectorial distribution of the gravitational field in a previous paper [13].

The axial diffusion time scale (L/u_c), where u_c is the characteristic velocity for natural convection and the diffusion time scale of the metal structures (W/α_m) were identified to dominate time scales for the prototype. Based on the axial diffusion time constant and on the characteristic velocity for natural convention, the following non-dimensional variables are defined:

$$x^* = \frac{x}{L} \ , \tag{4}$$

$$y^* = \frac{y}{D} \ , \tag{5}$$

$$y_w^* = \frac{y_w}{W} \ , \tag{6}$$

$$\vec{u}^* = \frac{\vec{u}}{\sqrt{(g\beta\Delta TD)}} \ , \tag{7}$$

$$t^* = \frac{t\sqrt{(g\beta\Delta TD)}}{L} \ , \tag{8}$$

$$T^* = \frac{T - T_\infty}{\Delta T} \ . \tag{9}$$

By making use of the divergence theorem, the momentum and energy equations are transformed in integral forms where the relative geometrical characteristics of model and prototype are preserved. The metal energy equation is integrated under the assumption of lumped heat capacity in the direction orthogonal to the wall. Therefore, it represents the axially local transient thermal behavior of the wall. Then one can readily identify the following non-dimensional parameters:

$$\Pi_1 = \frac{L}{D} \ , \tag{10}$$

$$\Pi_2 = (Gr)^{-1/2} \ , \tag{11}$$

$$\Pi_3 = (Pr)^{-1} \ , \tag{12}$$

$$\Pi_4 = \frac{\rho c}{(\rho c)_m}\frac{D}{W} \ , \tag{13}$$

$$\Pi_5 = \frac{h_e D}{k} \ . \tag{14}$$

There are two difficulties in applying this scaling criteria:

1. The wide range of temperatures obtained by the transient requires careful consideration of the variation of physical properties.
2. The elevated temperatures of the prototype require inclusion of the radiant heat transfer contribution.

The second problem is elevated by treating the gas as a non-Kirchoff surface heavier gas emissivity of 0.4 and absorptivity 1, which means that the portion of radiation transmitted to the gas layer further away from the metal surface is absorbed within the gas itself [13]. Therefore, the radiation contribution to the overall heat transfer coefficient is included. But the convective heat transfer coefficient is difficult to evaluate due to the lack of knowledge concerning the transient flow of steam in the hot leg.

In terms of the non-dimensional parameters the conservation equations are given as follows:

$$\frac{\partial u^*}{\partial t^*}\gamma_1 + u^{*2}\gamma_2 - \Pi_1\Pi_2(\frac{\partial u^*}{\partial y^*})_{@wall}\gamma_3 = \Pi_1\gamma_4 \ , \tag{15}$$

$$\frac{\partial T^*}{\partial t^*}\gamma_5 + u^*T^*\gamma_6 - \Pi_1\Pi_2\Pi_3\Sigma_h (\frac{\partial T^*}{\partial y^*})_{@wall}\gamma_7 = 0 \ , \tag{16}$$

$$\frac{dT_m^*}{dt^*} + \Pi_1\Pi_2\Pi_3\Pi_4\Sigma_h(\frac{\partial T^*}{\partial y^*})_{@wall} + \Pi_1\Pi_2\Pi_3\Pi_4\Pi_5 T_m^* = 0 \ . \tag{17}$$

Note that the temperature of the hot leg metal wall is the parameter of interest. The solution of Equation 17 has the form:

$$T_m^* = e^{-t^*/\tau}[\int_0^{t^*} e^{z/\tau} f(T^*)dz + C] \ , \tag{18}$$

where:

$$\tau = (\Pi_1\Pi_2\Pi_3\Pi_4\Pi_5)^{-1} \ , \tag{19}$$

$$f = 1 + \frac{e^{-t_f^*/\tau} - 1}{t_f^*/\tau} \ , \tag{20}$$

where the relative magnitude of the system time constant and the hot leg time constant can be obtained as:

$$\frac{\tau_{system}}{\tau_{hotlegwall}} = \Pi_1\Pi_2\Pi_3\Pi_4\Pi_5 \ . \tag{21}$$

Scaled model generated experimental data can be transposed to prototypical conditions using the following relations:

$$t_{prototype} = (\frac{L}{\sqrt{(\beta\Delta TD)}})_{p/m} t_{model} \ , \tag{22}$$

$$(T_m - T_\infty)_{prototype} = (\Delta T)_{p/m}(T_m - T_\infty)_{model} \ . \tag{23}$$

PHENOMENOLOGY

The horizontal portion of the hot leg has been more closely examined because the counter-current single phase flow (SF_6) in the hot leg sleeve is observed and the flow associates the energy and mass transport to the hot leg and the surge line in order to evaluate the amount of energy carried by the fluid into each hot leg. The counter-current flow in the horizontal portion of the hot leg has been closely scrutinized.

The upper and the lower segments in the horizontal portion of the hot leg are considered for the hot and cold fluid, respectively. The hot fluid is driven from the pressure vessel to the vertical portion of the hot leg and the cold fluid follows from the vertical portion of the hot leg to the pressure vessel. In fact, the net energy which is carried by the fluid is mostly provided to the hot leg metal wall (i.e., the metal wall at the surge line), where the failure is expected.

There are three methods to calculate the average velocity in the hot and the cold segments as follows:

1. The velocity profiles are discerned from the temperature profiles (measured by ten TCs located in the radial position where five are in the upstream, close to the reactor pressure, and another five are in downstream) which are, by utilizing principles of momentum conservation, assuming a laminar, quasi-steady state flow. The energy balance equation becomes as follows:

$$\rho C_p(\frac{\partial T}{\partial t} + u\frac{\partial T}{\partial x} + v\frac{\partial T}{\partial y}) = \kappa(\frac{\partial^2 T}{\partial x^2} + \frac{\partial^2 T}{\partial y^2}) \ , \tag{24}$$

with the prior assumptions, as well as the Boussinesq approximation, therefore, the

temperature gradient in the axial direction (x) is very small. Hence, the second partial derivative, with respect to the axial direction, approaches zero, then we arrive at the following relation as:

$$u\frac{\partial T}{\partial x} = \alpha\frac{\partial^2 T}{\partial y^2} \ . \tag{25}$$

Note that the distance between the TCs in the axial direction of the horizontal portion of the hot leg is 10 cm, so a partial derivative is of course, nonsensical. We make, therefore, a further assumption as follows:

$$\frac{\partial T}{\partial x} \approx \frac{\Delta T}{\Delta x} \ . \tag{26}$$

By implication that this is more or less constant, we are left with the following equation:

$$u = \frac{\alpha}{\frac{\Delta T}{\Delta x}}\frac{\partial^2 T}{\partial y^2} \ . \tag{27}$$

Note that the velocity sign depends on the gradient of the temperature in the axial direction and the second derivative of temperature in the radial direction (y-direction). Here we consider an experimental case where the pressure of the system is 1.5 bars and the operating power is 47 kW. At 2703 seconds the maximum and the average velocity in the hot segment is 2.9 cm/s and 1.8 cm/s, respectively, and 18.2 J energy is also carried through the hot segment in one second (Figure 2). But in the cold segment, the maximum and the average velocity are -1.5 cm/s and -1.1 cm/s, respectively, where 11.6 J energy is extracted from the cold segment to the reactor in a second. Hence, the total net energy of 6.6 J is contributed to the hot leg metal wall in one second.

2. Here we are interested to evaluate the average velocity by using the momentum balance in the hot and the cold segments. The buoyancy (inertial) force is considered here, in order to drive the fluid from the reactor to the hot leg, because of the density difference (natural convection) in the system. It was found that the hot segment is skewed toward the top in the horizontal portion of the hot leg and the boundary-line between two segments is inclined such that the inlet area of the hot segment is larger than the outlet area of the hot segment because of the buoyancy forces.

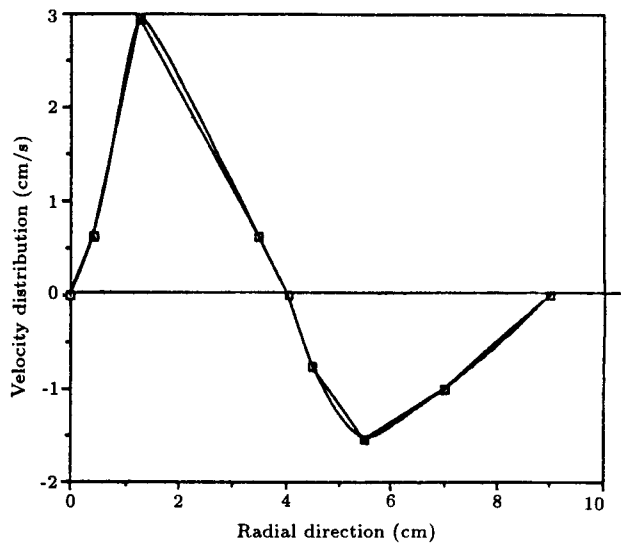

Figure 2. Velocity distribution in the horizontal portion of the hot leg in the radial direction.

For simplicity, we assume that there is no mass and energy interchanged between the two segments and the horizontal part of the hot leg, considered as the rectangular channel, which is pondered as a control volume. The turbulent shear stresses are applied between fluid and the channel walls, but the laminar shear stresses between the two segments are imposed. For the steady state case, the momentum balance for each segment and the continuity relation between the two segments are as follows:

$$A_{1h}[\bar{P}_{1h} + \frac{1}{2}\rho_h \bar{u}_{1h^2}] - A_{2h}[\bar{P}_{2h} + \frac{1}{2}\rho_h \bar{u}_{2h^2}] - F_{wall,h} - F_{interfacial} = 0 \ , \tag{28}$$

$$A_{2c}[\bar{P}_{2c} + \frac{1}{2}\rho_c \bar{u}_{2c^2}] - A_{1c}[\bar{P}_{1c} + \frac{1}{2}\rho_c \bar{u}_{1c^2}]$$

$$- F_{wall,c} - F_{interfacial} = 0 \ , \tag{29}$$

$$\rho_h A_{1h} \bar{u}_{1h} = \rho_c A_{1c} \bar{u}_{1c} \ , \tag{30}$$

where the subscripts $1h$ and $2h$ refer to the inlet and the outlet area of the hot segment (upper portion), respectively, but subscripts $1c$ and $2c$ refer to the outlet and inlet area of the cold segment (lower portion) in the channel, respectively. By doing some manipulation and the substitution of Equations 29 and 30 into Equation 28, one could obtain a relation for the hot fluid velocity at the inlet channel as follows:

$$a\bar{u}_{1h^2} + b\bar{u}_{1h} + c = 0 \ ,$$

where:

$$a = \frac{1}{2}\rho_h \frac{H_{1h}}{H}[(1 - \frac{H_{1h}}{H_{2h}}) + (\frac{\rho_h}{\rho_c}\frac{H_{1h}}{H_{1c}})(\frac{H_{1c}}{H_{2c}} - 1)] \ , \tag{31}$$

$$b = 32L^2 H_{1h}(\frac{\mu_h}{H_{Ah}^3} + \frac{\rho_c \rho_h}{H_{Ac}^3 \mu_c}) + \frac{5.7}{H}(\frac{H_h}{H_{AH}} + \frac{H_{1h}\rho_h}{H_{Ac}\rho_c})[(\rho_h \mu_h L u_{add})^{\frac{1}{2}} + (\rho_c \mu_c L u_{add})^{\frac{1}{2}}] \ , \tag{32}$$

$$c = \frac{1}{2}\rho_h g \beta \Delta T \Delta H \ , \tag{33}$$

$$u_{add} = u_{Ah} + u_{Ac} \ . \tag{34}$$

The parameters in the above equations have their usual meanings.

We consider the similar experiment applied to the previous section where the pressure of the system is 1.5 bars, $\Delta T = 50^{\circ}$ C and $\Delta H = 1$cm hence, the hot and cold fluid average velocities are 9 cm/s and -5 cm/s (opposite direction), respectively. These results are three times larger than those obtained from part 1. Hence, the analytical method for evaluating the counter-current average velocities of the hot and the cold segments in the horizontal portion of the hot leg, comparatively, provide good results in regard to the experimental data evaluations for the counter-current velocities.

3. The cross correlation method could also be applied in order to obtain the counter-current velocities in the horizontal channel. First, one could filter the obtained data from the experiment by adding the two adjacent transient temperature data related to the upstream and downstream of the horizontal channel. Then the Fast Fourier Transform (FFT) is used to acquire the spectrum and the phase shift with respect to the frequency in order to estimate velocities of the hot fluid and the cold fluid in the channel. This method has not yet been applied.

Energy balances (based on the experimental data) show that a relatively small amount of the core power is deposited in the hot legs. Two transient energy balances are shown in Table 2. The energy deposited in the fluid and in the hot legs represents about 5 percent of the total power input. Hence, the hot leg metal wall could reach to the failure point at the pressurizer surge line for 5 percent fraction of total power.

DISCUSSION AND SCALED RESULTS

The goal in this section is to infer the temperature rise at prototypical conditions from the scaled SF_6 experimental data measured at the core top and the hot leg metal wall near the surge line. By modifying Equations 22 and 23 one can obtain:

$$(T_m - T_\infty)_{P/m} = \left[\left(\frac{L}{\sqrt{\beta D}}\right)_{P/m}\right]^{2/3} \star R^{2/3} \ , \tag{35}$$

$$t_{P/m} = \left[\left(\frac{L}{\sqrt{\beta D}}\right)_{P/m}\right]^{2/3} \star R^{-1/3} \ , \tag{36}$$

where:

$$R = \frac{(\frac{dT}{dt})_{prototype}}{(\frac{dT}{dt})_{model}} \ . \tag{37}$$

R is thus a temperature ramp ratio which can serve as a bridge between prototypical

Table 2. Transient energy deposition (percentages).

	Core Power 37 kW (t_m = 135 s)	**Core Power 37 kW (t_m = 635 s)**
Vessel Metal	36	46
Internal Metal Masses	37	22
Heaters	17	11
Cold Legs Metal	5	13
Hot Legs Metal	3	5
Losses to Ambient	0	2
Fluid (i.e. SF_6)	2	1

and scaled facility conditions. It also serves as a parameter which provides a trade-off between conflicting requirements of accuracy and experimental measurement range as shown in Table 3. The data in Table 3 are evaluated for ramp ratios equal to 1, 2, 5, 10 and 20 in order to illustrate its effect on the magnitude of the distortions (the hot legs average distortions) with an assumed convective heat transfer coefficient of 100 $W/m^{2^\circ}C$. Inspection of this table shows that the geometrical scale leads to a decrease in the area to volume ratio in the hot legs and to a reduction of the natural convection driving force due to the reduction in elevation. The net result is an increase in the significance of the viscous term in the model. The presence of the radiation contribution in the prototype enhances the overall heat transfer coefficient and mitigates the distortion due to the geometric scale. The additional section of the hot leg wall thickness further reduces the distortion in the metal time constant.

Note that, for a unit ramp ratio, the time ratio and the temperature scale ratio must be identical. For low ramp ratios, the scaling invariant ratios are closer to unity. However, the time ratio is larger, which implies that the experimental transient is short. Furthermore, to achieve such small ramp ratios, a steep experimental temperature increase is required (i.e., large power inputs). Hence, the simulated prototypical temperature range is limited to the initial portion of the heat-up transient. Large ramp ratios provide good coverage of

Table 3. Effect of the ramp ratio on the hot legs average distortions.

Ramp ratio	R = 1	R = 2	R = 5	R = 10	R = 20
Time: $(t)_{p/m}$	3.64	2.89	2.13	1.69	1.34
Reference temperature difference: $(\Delta T)_{p/m}$	3.64	5.78	10.64	16.89	26.82
Aspect ratio: $(\Pi_1)_{p/m}$	1.24	1.24	1.24	1.24	1.24
Viscous term: $(\Pi_1\ \Pi_2)_{p/m}$	0.19	0.15	0.11	0.09	0.07
Fluid-wall heat transfer: $(\Pi_1\Pi_2\Pi_3\Sigma_h)_{p/m}$	0.26	0.21	0.15	0.12	0.10
Metal wall time constant: $[(\Pi_1\Pi_2\Pi_3\Pi_4\Pi_5)^{-1}]_{p/m}$	0.88	0.70	0.52	0.41	0.33

the prototypical conditions, simulating sharp temperature ramps with limited power and good experimental qualification, since the time ratio is reasonably small. If a temperature excursion for the prototype of 1000° C is assumed, one should run the experiment from ambient temperature (25° C) up to 300° C. The test duration depends on the prototypical ramp, where typical ramp values range from 0.5 to 2° C/s. A unit ramp ratio seems to constitute a reasonable compromise between the two conflicting requirements of range and accuracy.

The experimental bounds are for system pressure less than 20 bars and a temperature of 500° C. The tests are interrupted when the core heaters reach this limiting temperature. Within these limitations, the tests are conducted by increasing the power of the core from a steady state initial condition at ambient temperature. The pressure is held at about 20 bars throughout the test and, upon reaching the maximum temperature set point, the core heaters are automatically tripped. The UMCP facility has been operated with core power in the range between 27 and 57 kW. The test durations are from less than ten minutes up to one hour.

Figure 3 shows for different model temperature ramps (° C/s) where the transient temperature of the fluid measured at the top of the core increases more rapidly for the larger model temperature ramp (0.46° C/s) at a shorter time. The top of the core has been selected since it is representative of the highest bulk fluid temperature. Note that each of the four traces represent multiple tests. The figure illustrates that the tests are repeatable and the temperature trajectories are well bounded. This model temperature ramp at the top of the core is used in the scaling to calculate the ramp ratio. The warm up period for these tests is about five minutes. Hence, substantial convective motion takes place. The tests having a duration of less than five minutes are not relevant since there is no time for convective flow to initiate.

The temperature of the metal at the surge line location for the same four temperature ramps is shown in Figure 4. Note that as the power is increased (i.e., higher temperature ramps), the magnitude of the temperature excursion at the surge line decreases.

In order to calculate the ramp ratio, a prototypical temperature ramp must be postulated. The metallurgical analysis performed by Hobbins [17] shows maximum temperatures

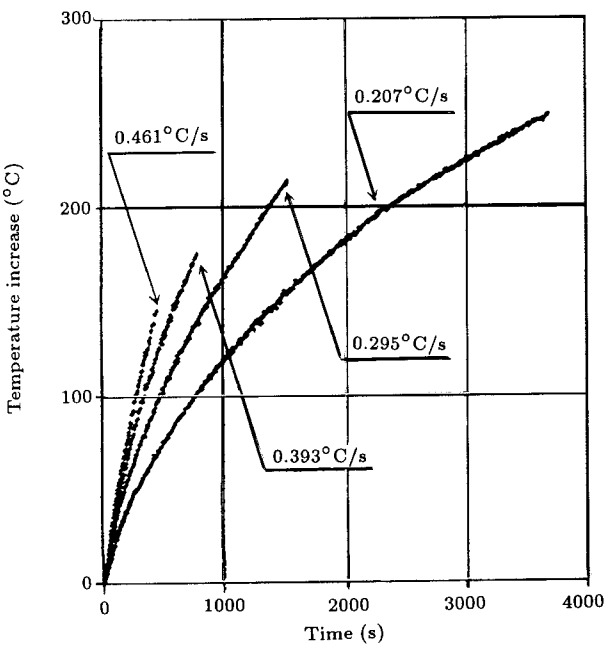

Figure 3. Temperature increase at the top of the core in the model for various temperature ramps.

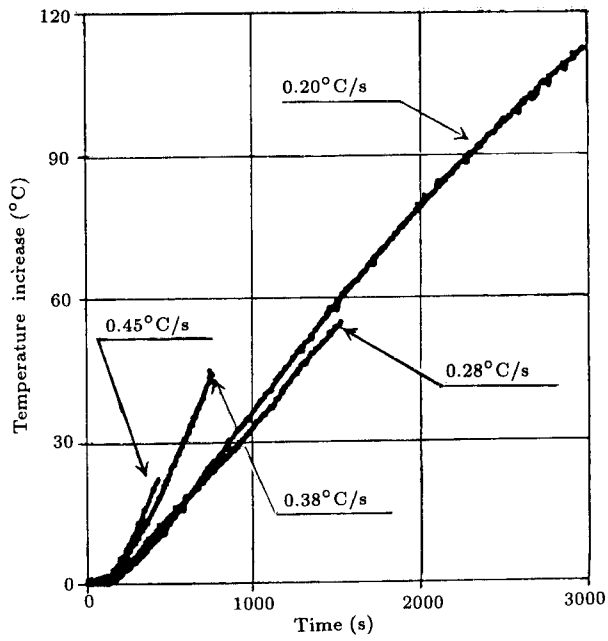

Figure 4. Temperature increase at the surge line metal in the model for various temperature ramps.

in the metal at the top of the core of about 1000°C. The initial condition can be assumed to be about 300°C and the TMI-2 transient has taken place in 2100 seconds [18,19]. This corresponds to a prototypical temperature ramp in the metal of 0.33°C/s. By assuming that the fluid temperature ramp is three times the one of the adjacent metal, a prototypical temperature ramp of 1.0°C/s is postulated. Since there is uncertainty in this estimate, results for half and twice this value are shown (i.e. : 0.5, 1.0, 2.0°C/s).

Careful study of Figures 5, 6 and 7 based on different prototypical ramps (i.e., 0.5, 1.0 and 2.0°C/s) and different ramp ratios, illustrate that, for the higher prototypical ramp of 2°C/s, the prototypical temperatures rise for the fluid measured at the top of the core and reach 2100°C for a ramp ratio of 10 in 35 minutes. These traces are evaluated independently from the four model transients conducted at different powers (i.e., with different ramp ratios) which demonstrates the effectiveness of the scaling laws. Also, it is observed that, for the bigger distorted ramp ratio, the temperature rise is considerable with respect to the temperature rise obtained for the smaller distorted ramp ratios.

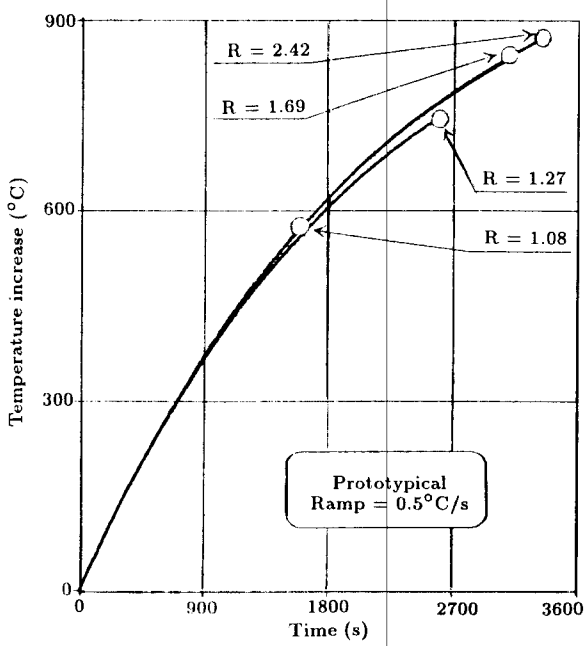

Figure 5. Prototypical temperature increase at the top of the core for various ramp ratios and for a postulated temperature ramp of 0.5°C/s.

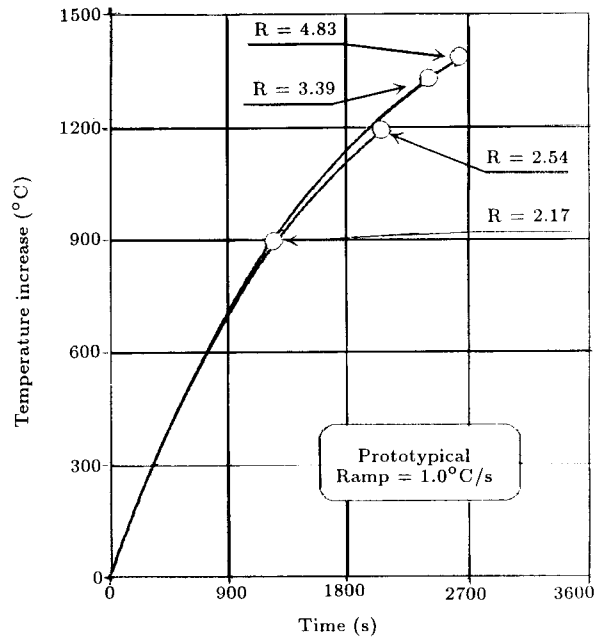

Figure 6. Prototypical temperature increase at the top of the core for various ramp ratios and for a postulated temperature ramp of 1.0°C/s.

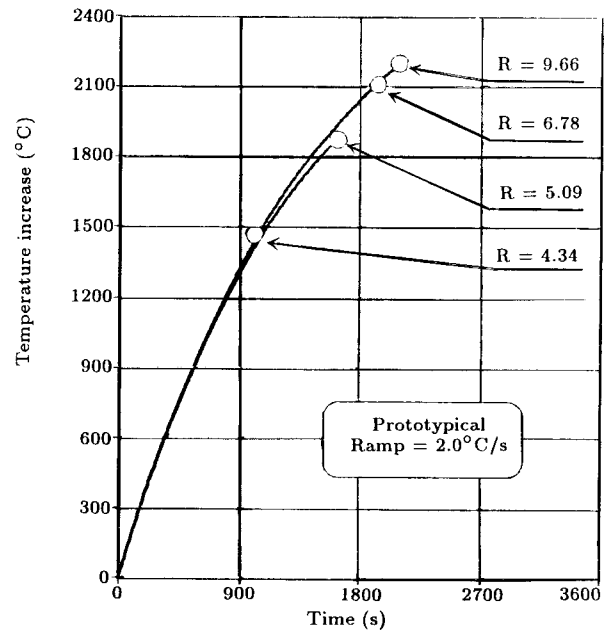

Figure 7. Prototypical temperature increase at the top of the core for various ramp ratios and for a postulated temperature ramp of 2.0°C/s.

Once confidence in the scaling procedure has been established, similarly, the predicted temperature rise of the hot leg metal wall at the pressurizer surge line nozzle, based on different prototypical and different ramp ratios, are shown in Figures 8, 9 and 10. An arbitrary failure threshold has been defined for a temperature increase of 1000°C which corresponds to 1300°C at the surge line nozzle metal. The slopes of the traces for various ramp ratios are different. This means that, for a prototypical ramp of 0.5°C/s, the temperature rise of the surge line metal reaches 1000°C by extrapolation where the failure is expected in 258 minutes. However, for the ramp ratio of 2.42, the temperature rise reaches 700°C in 150 minutes. For the prototypical temperature ramp of 1°C/s and the ramp ratio of 4.8, the temperature rise attains 1000°C in 133 minutes, but for the small ramp ratios, the temperature rises are much smaller. At last, for the prototypical ramp of 2°C/s and the ramp ratio of 6.78, the temperature rise of the hot leg metal wall at the surge line, where the failure is expected, attains 820°C in 47 minutes. If the larger prototypical temperature ramp and the ramp ratio are considered, the failure is expected in a shorter time.

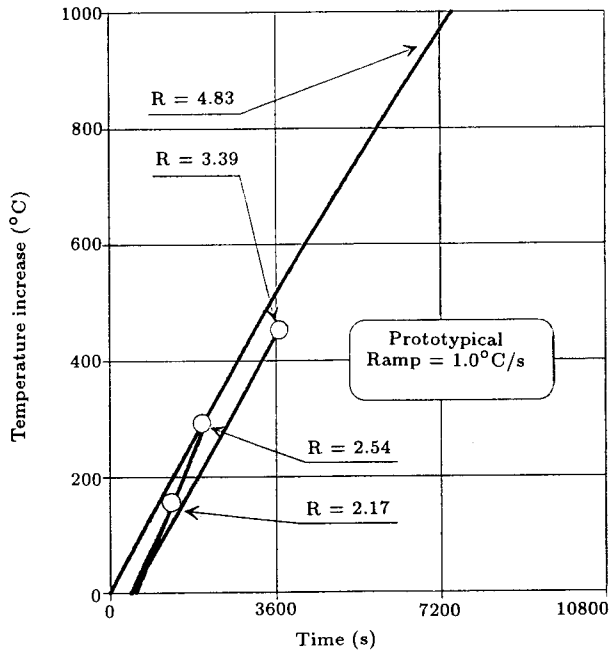

Figure 9. Prototypical temperature increase at the surge line metal for various ramp ratios and for a postulated temperature ramp of 1.0°C/s.

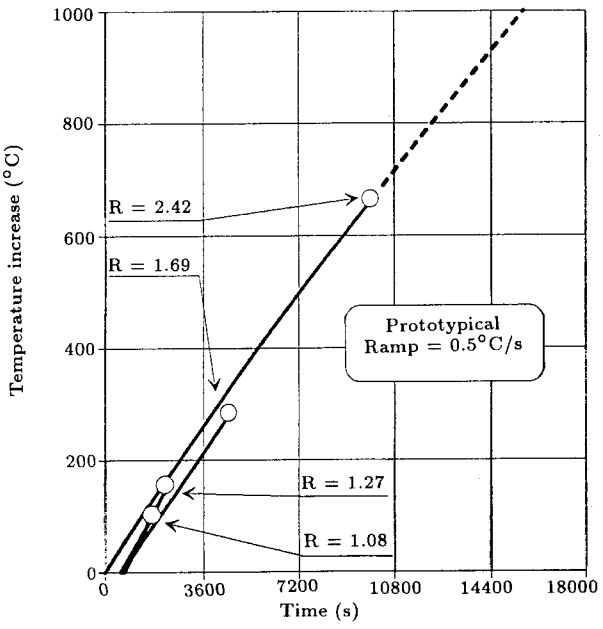

Figure 8. Prototypical temperature increase at the surge line metal for various ramp ratios and for a postulated temperature ramp of 0.5°C/s.

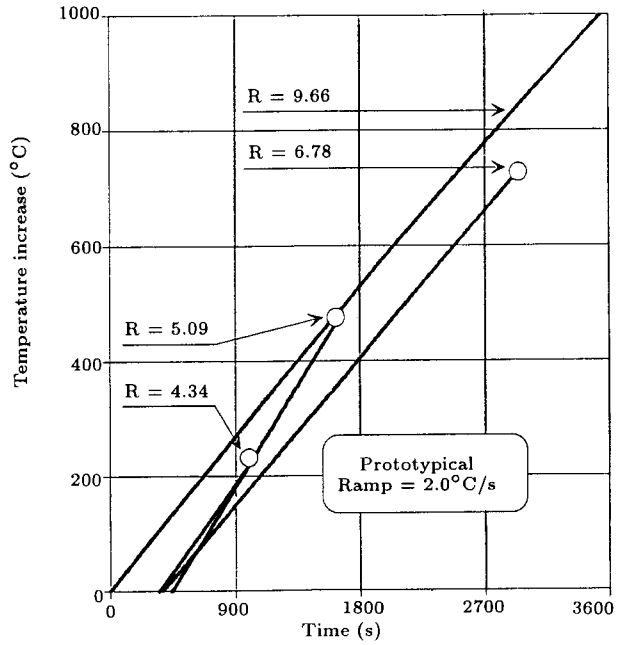

Figure 10. Prototypical temperature increase at the surge line metal for various ramp ratios and for a postulated temperature ramp of 2.0°C/s.

Figure 11 demonstrates the estimated time-to-failure (hours) for the hot leg metal wall at the surge line with respect to the prototypical temperature ramp (°C/s). The steepest transients and their prototypical extrapolation are considered here, since the earlier time to failure is the most critical. The natural circulation heat up segment of the TMI-2 transient lasted about 35 minutes and its postulated temperature ramp is of 1°C/s. The two dashed lines, corresponding to these values, meet in a region where the conditions are far from failure.

A postulated prototypical temperature ramp of more than 2°C/s or a transient of about 1.7 hours could be considered reasonably close to failure conditions at the surge line nozzle. Therefore, if the TMI-2 accident was prolonged, one could estimate that the failure at the surge line metal wall would be expected at about two hours for the prototypical temperature ramp of 1°C/s. While, for the prototypical temperature ramp of 2°C/s, the failure time could be anticipated at about one hour and for the prototypical temperature ramp of 0.5°C/s the anticipated failure time would be about four hours.

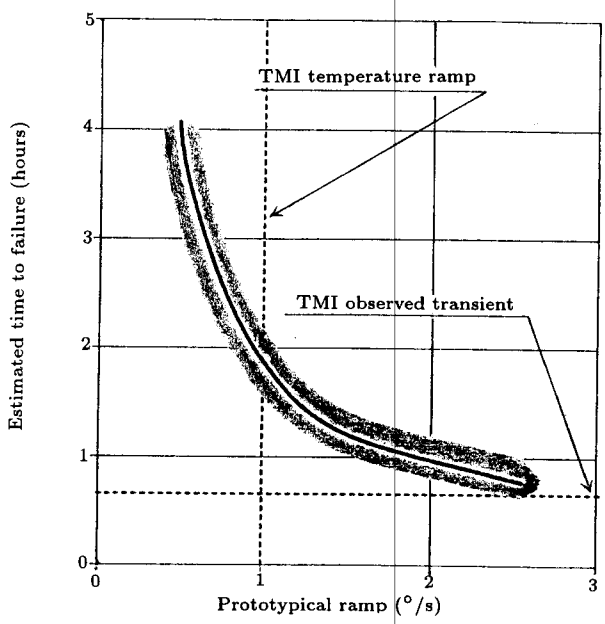

Figure 11. Estimated prototypical time-to-failure as a function of postulated prototypical temperature ramps.

CONCLUSIONS

Scaling of the hot legs, which is derived previously, is carried out and it provides a methodology which can be used to infer the transient thermal behavior of the hot leg metal wall in the proximity of the pressurizer surge line nozzle.

Three different approaches have been conducted for evaluating the fluid velocity at the horizontal portion of the hot leg in order to estimate the amount of energy carried by the fluid into the hot leg and the hot leg metal wall (i.e., the surge line). The energy deposited in the fluid and in the hot legs represents about 5 percent of the total power input.

The UMCP experiments are conducted in a geometrically scaled facility and use SF_6 to simulate a high pressure, high temperature steam-hydrogen mixture. Four sets of tests are conducted at different powers, yielding different temperature ramps at the top of the core. By postulating a prototypical temperature ramp of about 1.0°C/s and using a range of temperature ramp ratios, independent prototypical transient traces are obtained.

Figures are provided for a range of temperature ramp ratios and the prototypical temperature ramp about 1.0°C/s in order to evaluate the transient temperatures measured at the top of the core and the hot leg metal wall at the surge line from the test facility data. The estimated time to failure (hours) with respect to the prototypical temperature ramps ratio is also provided and compared with the estimated conditions during the TMI-2 severe accident transient. The TMI-2 transient is shown to be reasonably far from failure conditions. It is found that failure would have occurred for heat-up transients lasting almost three times as long, or for the prototypical temperature ramp of more than 2°C/s. For the prototypical temperature ramp of 2°C/s, the estimated time where the hot legs metal wall at the surge line fails in order to depressurize the reactor system, is about 65 minutes, and for the prototypical temperature ramp of 1°C/s, the estimated time to failure will be about two hours.

NOMENCLATURE

A	area
c	heat capacity
D	inside diameter
f	internal metal structure heat up fraction
F	shear force
g	gravitational acceleration
Gr	Grashoff number
h	heat transfer coefficient
H	channel height
J	Joule
k	thermal conductivity
L	length
n	unit vector normal to the wall
P	pressure
Pr	Prandtl number
q	heat flux
R	temperature/time ramp ratio
t	time
T	temperature
u	velocity
W	wall thickness or characteristic length of a metal structure
x	axial coordinate
y	fluid coordinate normal to the wall
y_w	metal coordinate normal to the wall
z	dummy variable
κ	thermal conductivity
β	thermal expansion coefficient
γ	gravitational field vector distribution
γ_i	integrated distribution (the integrated momentum and energy equations)
ΔH	twice the height difference between the inclined line with the horizontal line
ΔT	reference temperature difference
μ	viscosity
ν	kinematic viscosity
Π	non-dimensional parameter
ρ	density
σ	Stefan-Boltzmann constant
Σ_h	radiation enhancement
τ	time constant

Subscripts

A	average
add	summation
c	cold fluid
e	effective
h	hot fluid
inf	ambient
m	metal
p/m	prototype-to-model ratio
w	wall
$\star$	non-dimensional property
1	channel upstream surface in the horizontal hot leg
2	channel downstream surface in the horizontal hot leg

Superscript

$-$	average

REFERENCES

1. Allison, C.M. "Perspectives on in-vessel behavior as it affects DCH and DCH experiments", DCH Workshop, Annapolis, MD (1989).
2. Sheron, B.W. "Introduction and purposes", DCH Workshop, Annapolis, MD (1989).
3. Seghal, B.R. "Industry perspectives on DCH issue", DCH Workshop, Annapolis, MD (1989).
4. Dalmann, J. "Positive and negative aspects of depressurization", DCH Workshop, Annapolis, MD (1989).
5. Denny, V.W. "The role of natural circulation in severe accident analysis", *Proc.*

of the Topical Meeting on Reactor Physics and Safety, NUREG/CP-0080, **2** (1989).

6. Stewart, W.A., Pieczynski, A.T. and Srinivas, V. "Experiments on natural circulation", PWR Natural Circulation Meeting, Rockville, MD (1988).
7. Stewart, W.A. "Experiment on natural circulation during PWR severe accident", PWR Natural Circulation Meeting, Rockville, MD (1991).
8. Hansen, D.J. et al. "Depressurization as an accident management strategy to minimize the consequences of DCH", NUREG/CR-5447 (1990).
9. Bayless, P.D. "Analysis of natural circulation during a surry station blackout using SCADAP/RELAP5", NUREG/CR-5214 (1988).
10. Wassel, A.T., Ghiaasiaan, S.M., Denny, V.E. and Traci, R.M. "Modeling of natural circulation in reactor coolant system", *Fluid Physics Ind.*, FPI R88-05-04 (1988).
11. Tung, V.X. "Scaling review of the Westinghouse apparatus and natural circulation experiments", PWR Natural Circulation Meeting, Rockville, MD (1991).
12. No, H.C. and Ishii. "An analytical method for generating the scaling criteria of core uncovery and heatup processes", *ANS Proc. HTC*, **5**, pp 303-310 (1991).
13. di Marzo, M., Heper, H. and Almenas, K. "Scaling for the primary system transient heating in a severe accident scenario", National Heat Transfer Conference, San Diego, CA (1992).
14. Ostrach, S. *COMMIX Code Review*, LDS-3-90, Report to NRC- L.M. Shotkin (1990).
15. Hepper, H., di Marzo, M., Almenas, K., Abdelkader, S., Carter, E., Gopalnarayanan, S., Green, J., McNair, T. and Tafreshi, A. "Natural circulation induced heating of primary system components", University of Maryland Report, 031192 (1992).
16. Tafreshi, A. "Instrumentation design and data acquisition for a thermal conjugate transient", MS thesis, UMCP, College Park, MD (1992).
17. Hobbins, R.R. "INEL metallurgical studies", PWR Natural Circulation Meeting, Rockville, MD (1991).
18. Schlenker, L.D. "TMI-2 severe accident natural circulation scenario", PWR Natural Circulation Meeting, Rockville, MD (1991).
19. Bessette, D. "Characteristics of the TMI accident", PWR Natural Circulation Meeting, Rockville, MD (1991).